g

Chapter 1

Offset separation

The MZO operator presented in the preceding chapter can be formulated to allow for separate migration of each common-offset section. Several issues have to be taken into account for an optimal implementation of MZO in common-offset sections. Among the most important is the introduction of artifactsg in the offset domain. A second issue is how to speed up the algorithm using a stationary-phase approximation to the inner kernel. The MZO form in equation (??) is similar to the DSR equation, and the implementation for separate common-offset sections is analogous for the two algorithms. An accurate implementation for DSR is discussed in Popovici (1993), and the same techniques can be applied to eliminate artifacts in the MZO algorithm. At the end of this chapter, I also present analytical formulations for applying the DMO operator both after and before the normal-moveout correction (NMO).

1.1 Offset separation

The phase-shift formulation of the MZO presented in the preceding chapter in equation (??) is

$$p_0(t_0,k_y)=\int dk_h \int d\omega\; e^{-i\frac{\omega t_0}{2}\left[\sqrt{(1-Y)^2-H^2}+\sqrt{(1+Y)^2-H^2}\right]} p(\omega,k_y,k_h).$$

Let us consider as an input to the MZO process a 3-D cube $p(t,y,h)$ where all the common-offset sections are zero except a single 2-D common-offset section $p_{h0}(t,y;h_0)$, corresponding to a half-offset h_0. The result is equivalent to introducing a Dirac δ function in offset coordinates. The first step is to Fourier transform the $p(t,y,h)$ field in time and midpoint coordinates. Next, Fourier transforming over the offset dimension yields

$$p(\omega,k_y,k_h)=e^{-ik_hh_0}p_{h0}(\omega,k_y;h_0),$$

where the scaling factor for the Fourier transform, though omitted, is understood. Substituting the wavefield $p(\omega,k_y,k_h)$ in equation (??), we can write the phase-shift

MZO as

$$\begin{aligned} p_0(t_0,k_y;h_0) &= \int d\omega \int dk_h \; e^{-i\omega_0(\omega,k_y,k_h)t_0} \; e^{-ik_h h_0} p(\omega,k_y;h_0) \\ &= \int d\omega \; p(\omega,k_y;h_0) \int dk_h \; e^{-i\omega_0(\omega,k_y,k_h)t_0 - ik_h h_0}, \end{aligned} \tag{1.1}$$

where $\omega_0(\omega,k_y,k_h)$ is the phase-shift term defined in equation (**??**),

$$\omega_0 = \frac{\omega}{2}\left[\sqrt{(1-Y)^2-H^2}+\sqrt{(1+Y)^2-H^2}\right].$$

Equation (1.1) can be used to migrate to zero-offset individual common-offset sections, as shown in Figure 1.1.

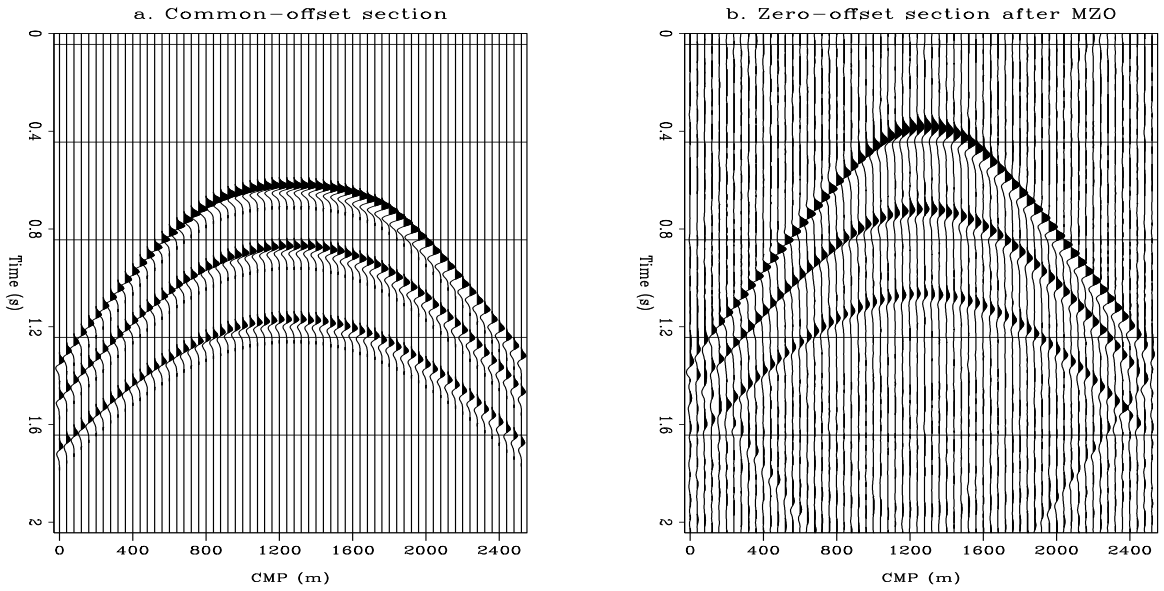

Figure 1.1: Single common-offset section and the output of MZO.
a. Common-offset section.
b. Zero-offset section obtained by applying MZO to the common-offset section. chapter2-C2f1wig [CR]

The speed of the algorithm is determined by the method used to compute the kernel

$$I(\omega,k_y;t_0,h_0) = \int dk_h \; e^{-i\omega_0(\omega,k_y,k_h)t_0 - ik_h h_0}. \tag{1.2}$$

Methods for fast evaluation of the stationary phase in equation (1.2) are discussed in Appendix 2.A.

Expression (1.1) also demonstrates the facts that separate common-offset sections can be migrated individually to zero-offset, and that there is no condition which requires all of them to be present in the 3-D prestack migration input data. When we process all the common-offset sections at the same time, the data field after Fourier transform along the offset axis becomes

$$p(\omega,k_y,k_h) = \int dh \; e^{-ik_h h} p(\omega,k_y,h),$$

which, when introduced into the MZO equation (??) allows for isolating the stacking step, which is the integration in the offset variable h:

$$\begin{aligned} p_0(t_0,k_y) &= \int d\omega \int dk_h \; e^{-i\omega_0(\omega,k_y,k_h)t_0} \int dh \; e^{-ik_h h} p(\omega,k_y,h) \\ &= \int dh \int d\omega \; p(\omega,k_y,h) \int dk_h \; e^{-i\omega_0(\omega,k_y,k_h)t_0 - ik_h h}. \end{aligned} \tag{1.3}$$

Without the stacking step, the migration to zero-offset for individual common-offset sections becomes

$$p_0(t_0,k_y,h) = \int d\omega \; p(\omega,k_y,h) \int dk_h \; e^{-i\omega_0(\omega,k_y,k_h)t_0 - ik_h h}. \tag{1.4}$$

It should be noted here that the integration boundaries for the integral in k_h are not infinite, and, moreover, do not correspond to the Nyquist values $\frac{-\pi}{dh}$ and $\frac{\pi}{dh}$ in the discrete case, but are given by the condition that the phase ω_0 be real. The problem is similar to that encountered in the prestack migration of individual common-offset sections (Popovici, 1993). As in the case of the DSR equation, using the wrong integration boundaries introduces artifacts into the MZO algorithm.

1.1.1 MZO artifacts

The DSR equation has the same form as the MZO equation. A comparison of the two integral equations reveals the mathematical similarities and suggests solutions for a better implementation of MZO. The DSR prestack migration equation has the form

$$p(t=0,k_y,h=0,z) = \int dk_h \int d\omega \; e^{-\frac{i\omega}{v}\left[\sqrt{1-(Y-H)^2}+\sqrt{1-(Y+H)^2}\right]z} p(\omega,k_y,k_h,z=0),$$

while the MZO equation is

$$p(t_0,k_y,h=0,z=0) = \int dk_h \int d\omega \; e^{-\frac{i\omega}{v}\left[\sqrt{(1-Y)^2-H^2}+\sqrt{(1+Y)^2-H^2}\right]\frac{t_0}{2}} p(\omega,k_y,k_h,z=0).$$

Both equations perform an integration in k_h and ω, and both have a double-square-root phase. Moreover, each square root contains the difference between two squared amounts.

An argument commonly used to explain the artifacts in DSR migration is that they are caused by Fourier domain wraparound along the offset axis. I have found that the artifacts can be minimized by varying the sampling along the offset-wavenumber axis, while respecting the existence boundaries required by the double-square-root phase.

Figure 1.2a shows the output of constant sampling in k_h DSR migration applied to a data cube (t, y, h) containing a single spike in a common-offset section with a half-offset $h_0 = 190m$. The shallower ellipse is an artifact. In contrast, the improved DSR migration in Figure 1.2b eliminated the shallow ellipse artifact. However, in a stacked section such artifacts are greatly attenuated because of the summing in offset that is implicitly done with the DSR equation. When each common-offset section is taken separately, as in common-reflection-point or AVO studies, the artifacts are a disturbing presence.

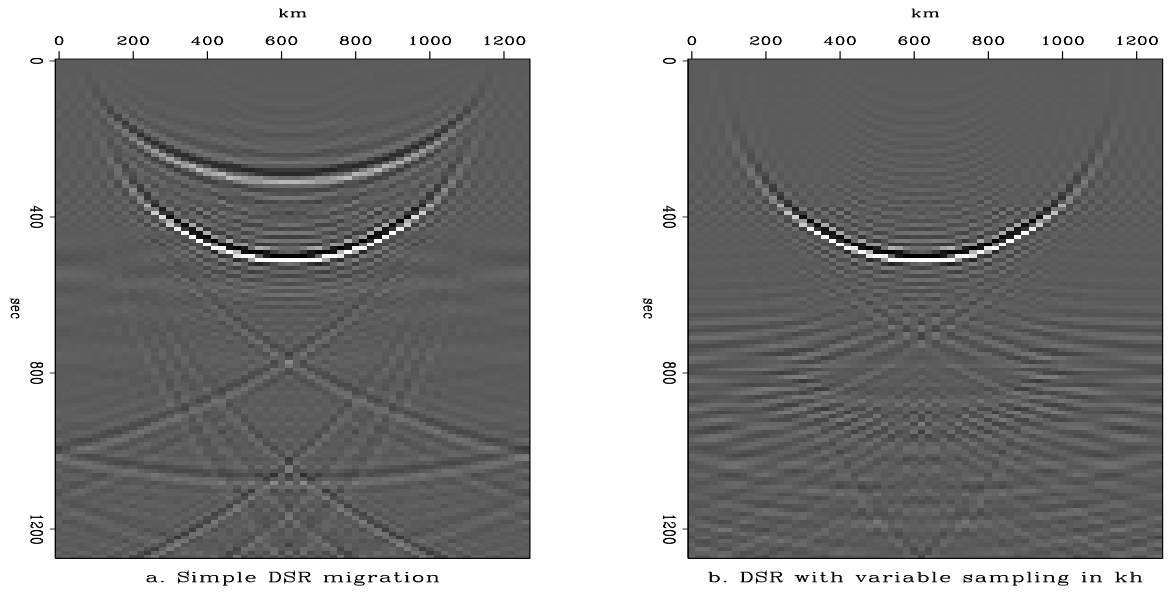

Figure 1.2: Output of DSR in offset-midpoint migration. The input cube contains a single spike for the common-offset section $h = 190m$.
a. DSR migration with constant k_h sampling. The shallower ellipse is an artifact.
b. DSR migration without offset artifacts. chapter2-C2f2 [CR]

The source of artifacts in DSR migration relates to equation (??), which limits the interval of existence for the variable k_h. Normally the offset wavenumber k_h is evenly sampled between the values $(-\frac{\pi}{dh}, \frac{\pi}{dh})$ in the DSR equation (??), which is necessary to perform the FFT along the offset axis. However, the requirement that the square-root expressions be real limits the available values for k_h.

A similar condition can be defined for the interval of existence of the variable k_h in the MZO phase (??), which must be real. This in turn requires that the two conditions

$$| \omega - v_y | \quad \geq \quad | v_h |$$

$$| \omega + v_y | \quad \geq \quad | v_h |$$

be satisfied simultaneously, where v_h and v_y are defined as

$$v_h = \frac{v k_h}{2}; \quad v_y = \frac{v k_y}{2}.$$

By examining all four possible sign cases for the given values of ω and v_y, represented in Figure 1.3, we can reduce the two conditions to a single condition:

$$|| \omega | - | v_y || \geq | v_h | . \tag{1.5}$$

The shaded area in Figure 1.3 represents the interval of existence for the variable v_h for each pair (ω, v_y).

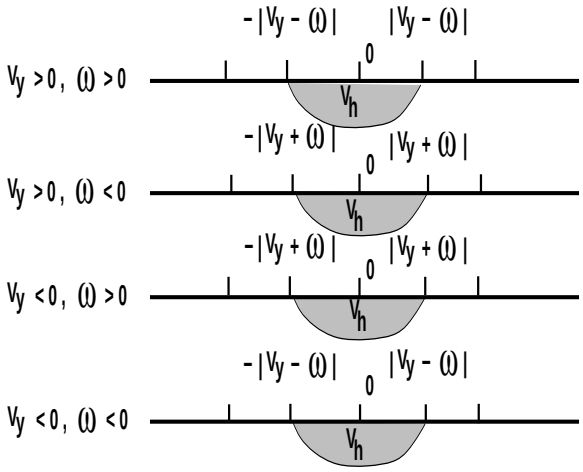

Figure 1.3: Four possible cases for the values of v_y and ω and the interval of existence of v_h. For each case the equation $|| \omega | - | v_y || \geq | v_h |$ satisfies the existence condition for v_h. chapter2-MZObound [NR]

A straightforward implementation of the MZO equation (1.4) produces significant artifacts. When, from the whole set of discrete values, only a subset of the values of k_h is used, artifacts appear in the phase expression. The integration in k_h is in fact an inverse Fourier transform along the offset axis, followed by extraction of the zero values in the offset variable. The inverse Fourier transform takes into account not only the domain of existence of the value k_h given by equation (1.5), but the whole domain of definition between the Nyquist values of k_h,

$$k_h \in \left[-\frac{\pi}{dh}, \frac{\pi}{dh} \right].$$

The region of integration can be much smaller than the domain in which k_h is sampled. As a result, only several discrete values of k_h are used to evaluate the inverse Fourier integral. The missing offset-wavenumbers set the value of the phase to zero for the discrete values of k_h that do not satisfy equation (1.5). The inverse Fourier transformation of the exponential shows very different results, as illustrated in Figure 1.4.

A careless implementation of the migration to zero-offset equation (1.4) will produce artifacts similar to the ones in the DSR migration with constant k_h sampling. Figure 1.5a shows the output of MZO applied to a data cube (t, y, h) containing a single spike in a common-offset section with a half-offset $h_0 = 500m$. In Figure 1.5b, the artifacts are reduced by using variable sampling for k_h.

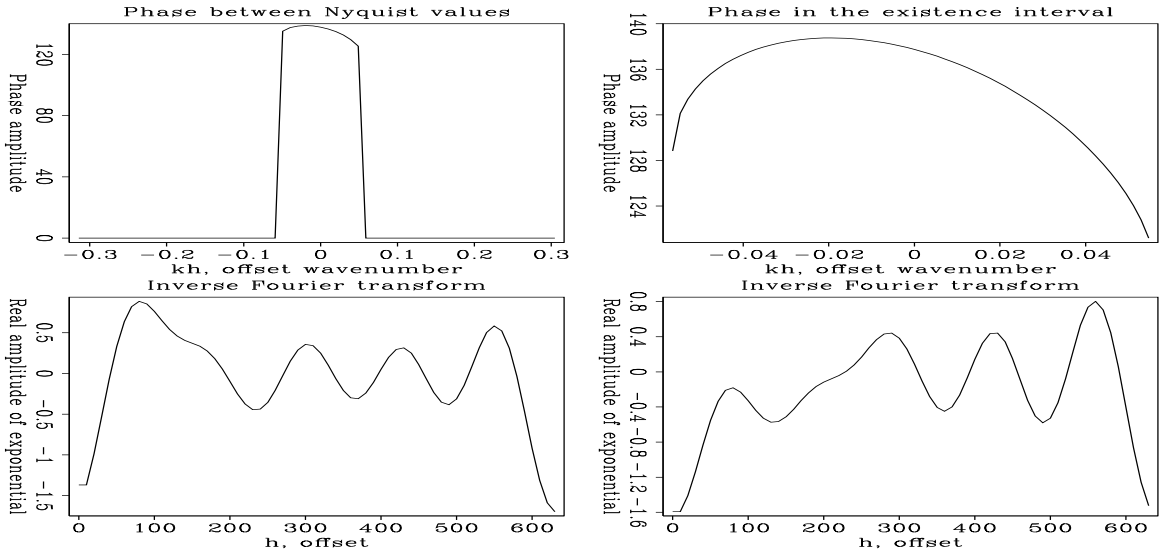

Figure 1.4: Comparison of the DSR phase defined between Nyquist values and between the more restrictive existence boundaries.
a. Phase and the inverse Fourier transform of the exponential, between Nyquist values.
b. Phase and the inverse Fourier transform of the exponential, in the strict existence interval. The values are the same as in the left figure, but sampled in the exact existence interval. chapter2-C2f3 [NR]

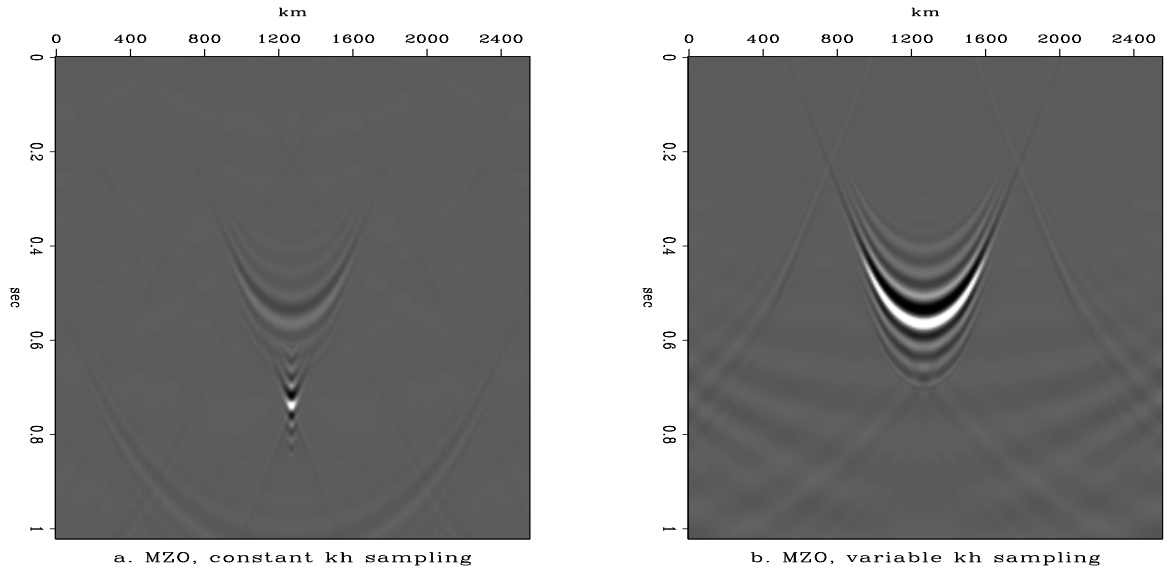

Figure 1.5: Output of MZO applied to an input cube containing a single spike in a separate common-offset section. The half offset used is $h = 500m$.
a. MZO using constant sampling in k_h. The deeper event is an artifact.
b. MZO using variable sampling in k_h. Offset artifacts are reduced. chapter2-C2f4 [CR]

1.1.2 MZO code structure

The basic migration to zero-offset algorithm which implements equation (**??**), and used to generate Figure 1.1b, can be summarized in pseudocode as

FFT along all axes $p(t,y,h) \rightarrow P(\omega,k_y,k_h)$
do $t0$
  do k_y
  do ω
  do k_h
  if $(\text{abs}(\frac{2}{v}\text{abs}(\omega) - \text{abs}(k_y)) > \text{abs}(k_h))$ then
    $P(\omega,k_y,k_h) = P(\omega,k_y,k_h)e^{-i\omega_0 dt0}$
    $M(t0,k_y) = M(t0,k_y) + P(\omega,k_y,k_h)$
  endif

In order to perform an FFT along the offset axis, we must evenly sample the variable k_h between the Nyquist negative and positive values. However, the existence condition for k_h in equation (1.5) restricts the domain of definition for the variable k_h. For each pair of values ω, k_y, the loop in k_h will use either a subset or all of the possible k_h sampled values.

The MZO algorithm can be rewritten, extracting the multiplication with the wavefield $P(\omega,k_y,h)$ outside the k_h loop, as shown in equation (1.4). The new algorithm keeps the phase separate from the data field:

for any h
FFT along t,y axes $p(t,y;h) \rightarrow P(\omega,k_y)$
for all ω,k_y,k_h;$ph(\omega,k_y,k_h) = e^{-ik_h h}$
do $t0$
  do k_y
  do ω
    do k_h
    $ph(\omega,k_y,k_h) = ph(\omega,k_y,k_h)e^{-i\omega_0 dt0}$
    $phase(\omega,k_y) = phase(\omega,k_y) + ph(\omega,k_y,k_h)$
  $M(t0,k_y) = M(t0,k_y) + P(\omega,k_y) * phase(\omega,k_y)$

The loop in k_h becomes a mere numerical integration of the exponential term, an integral that can be asymptotically approximated through the use of the stationary phase as explained in Appendix 2.A. Moreover, to minimize the artifacts in the offset domain, the variable k_h is sampled differently for each pair of values (ω,k_y). The interval of existence (1.5) for each pair (ω,k_y) is divided by the total number of k_h variables.

For depth-variable velocity, we have to sum the phase terms corresponding to each time $dt0$ level. The summation in time is done for individual values of the variable k_h. In other words, for depth-variable velocity, the exponential term contains the integral over time $t0$ of the phases corresponding to previous depth levels, separated for each value of k_h. Because we need to know the integral in time for each value of k_h, we cannot simply store the global value of the stationary phase approximation for each time increment. Knowing the stationary phase for a time level is not enough to carry the computation to the next time level, though it could produce a good approximation (Biondo and Palacharla, 1994).

The result is a slow migration to zero-offset algorithm that migrates one common-offset section in almost the time necessary to migrate all common-offset sections. However, finding a good stationary phase approximation to the integral (1.2) can speed up the algorithm hundreds of times. The resulting algorithm can be expressed in pseudocode as

for any h
FFT along t, y axes $p(t, y; h) \rightarrow P(\omega, k_y)$
do $t0$
    do k_y
    do ω
    compute $phase$ fast
    $M(z, k_y; h) = M(z, k_y; h) + P(\omega, k_y) * phase$

In Appendix 2.A, I discuss different properties of the phase function and how the stationary phase can be computed numerically, together with the approximations needed for depth-variable velocity.

1.2 Geometric interpretation of the stationary phase condition

A better understanding of the physical meaning of wave-equation derived integrals can be achieved by examining the geometrical interpretation of the stationary point condition. Equations (**??**) and (1.1) have a raypath representation that can be derived from the stationary point condition. The MZO geometrical interpretation is closely related to the DSR geometrical interpretation. I present first the geometrical condition for the prestack migration DSR equation and second the geometrical condition for MZO.

1.2.1 Geometrical condition for DSR

Given the plane wave represented schematically on the left in Figure 1.6, where γ is the angle of the plane wave at the surface and also the vertical angle of the takeoff ray, in the depth model we have the relation

$$\sin\gamma = \frac{v\Delta t}{\Delta y}.$$

For the same Δt and Δy in the time section we have

$$\frac{\Delta t}{\Delta y} = \tan\theta = \frac{\sin\gamma}{v}.$$

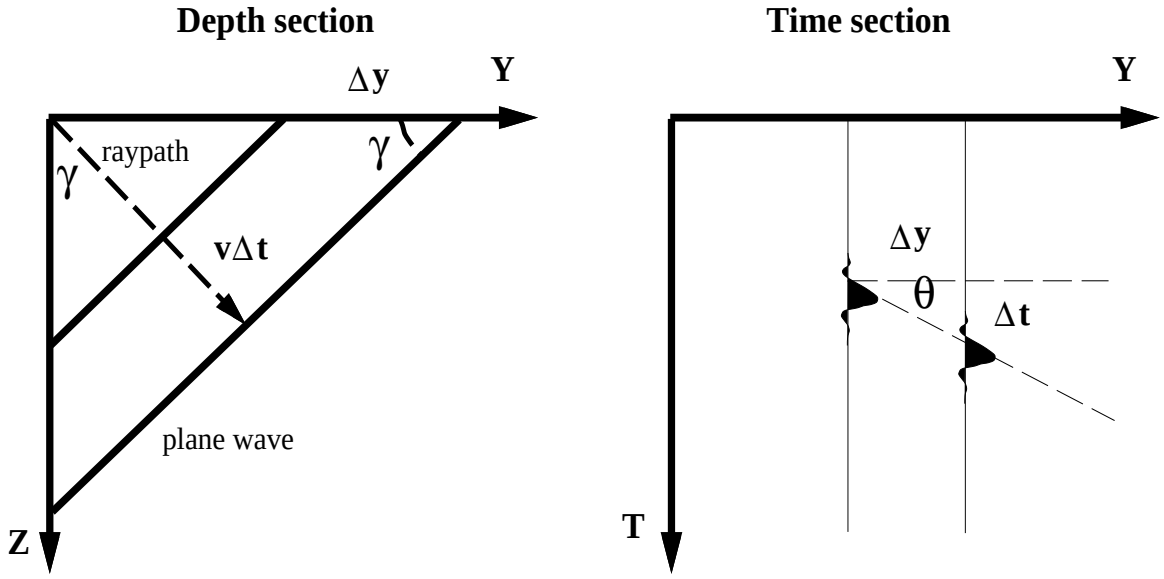

Figure 1.6: Plane wave in depth and time. chapter2-planewave [NR]

Another useful relation is the equation that relates the dip in a time section with the ratio of the Fourier coordinates. A segment of plane wave with slope $\frac{\Delta t}{\Delta y}$ is mapped in Fourier domain by a line with slope $\frac{k_y}{\omega}$:

$$\frac{\Delta t}{\Delta y} = \frac{k_y}{\omega} = \frac{2\sin\gamma}{v}, \tag{1.6}$$

where γ is the takeoff angle (measured from vertical). These relations will be used in analyzing the geometrical meaning of the stationary phase in prestack DSR migration, and MZO.

The DSR prestack migration equation has the form

$$p(t=0, k_y, h=0, z) = \int dk_h \int d\omega \; e^{ik_z z} p(\omega, k_y, k_h, z=0), \tag{1.7}$$

where the phase $k_z(\omega, k_y, k_h)$ was defined in the dispersion relation (??) to be

$$k_z(\omega, k_y, k_h) \equiv -\text{sign}(\omega) \left[\sqrt{\frac{\omega^2}{v^2} - \frac{1}{4}(k_y + k_h)^2} + \sqrt{\frac{\omega^2}{v^2} - \frac{1}{4}(k_y - k_h)^2} \right].$$

Substituting the explicit form of the Fourier transform over offset

$$p(\omega, k_y, k_h) = \int dh \; e^{-ik_h h} \; p(\omega, k_y, h).$$

in equation (1.7), and eliminating the stacking step, the prestack migration equation can be written as

$$p(t = 0, k_y, h, z) = \int d\omega \; p(\omega, k_y, h) \int dk_h \; e^{ik_z(\omega, k_y, k_h)z - ik_h h}. \tag{1.8}$$

The phase of the exponential in this case is

$$\phi(k_h) = -\text{sign}(\omega) z \left[\sqrt{\frac{\omega^2}{v^2} - \frac{1}{4}(k_y + k_h)^2} + \sqrt{\frac{\omega^2}{v^2} - \frac{1}{4}(k_y - k_h)^2} \right] - k_h h, \tag{1.9}$$

and in order to evaluate the stationary point we need to find the roots of the equation

$$\phi'(k_h) = -h + \text{sign}(\omega) z \left[\frac{k_h + k_y}{\sqrt{\frac{\omega^2}{v^2} - \frac{1}{4}(k_y + k_h)^2}} + \frac{k_h - k_y}{\sqrt{\frac{\omega^2}{v^2} - \frac{1}{4}(k_y - k_h)^2}} \right] = 0. \tag{1.10}$$

To find the geometrical meaning of this equation, we need to transform the offset and midpoint wavenumbers into shot and geophone wavenumbers, using the conversion relations:

$$\begin{aligned} k_y &= k_g + k_s \\ k_h &= k_g - k_s. \end{aligned}$$

Equation (1.10) becomes

$$[\frac{vk_g}{\omega} \frac{1}{\sqrt{1 - (\frac{vk_g}{\omega})^2}} - \frac{vk_s}{\omega} \frac{1}{\sqrt{1 - (\frac{vk_s}{\omega})^2}}] z = 2h, \tag{1.11}$$

or using the plane wave relation (1.6) and appropriate values for the angle signs, we have a geometrical relation, as follows:

$$[\frac{\sin\alpha}{\sqrt{1 - \sin^2\alpha}} - \frac{\sin\beta}{\sqrt{1 - \sin^2\beta}}] z = 2h,$$

where the angles α and β are the takeoff angles at the source and receiver, as shown in Figure 1.7. The stationary phase condition reduces to the provision that the horizontal projection of the source ray plus the horizontal projection of the receiver ray should be equal to the full offset:

$$z \tan\alpha - z \tan\beta = 2h.$$

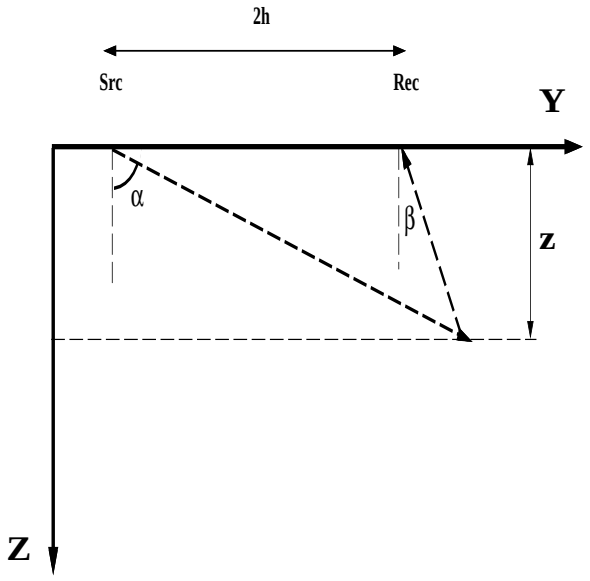

Figure 1.7: Geometric interpretation of the stationary phase condition for DSR prestack migration. chapter2-ShotRecgeo [NR]

For depth variable velocity, the dispersion relation is the sum of terms calculated for each depth interval:

$$\Delta z \left[\sum_i \tan \alpha_i - \sum_i \tan \beta_i \right] = 2h, \tag{1.12}$$

where the angles α_i and β_i are the vertical angles in each depth layer of the raypaths from the source and receiver.

1.2.2 Geometrical condition for MZO

The stationary phase condition for MZO is found in Appendix 2.A, equation (1.40) to be:

$$\frac{vt_0}{2} \text{sign}(\omega) k_h \left[\frac{1}{\sqrt{(\frac{2\omega}{v} - k_y)^2 - k_h^2}} + \frac{1}{\sqrt{(\frac{2\omega}{v} + k_y)^2 - k_h^2}} \right] = 2h.$$

Similar to the DSR geometric interpretation, the stationary condition can be converted into a geometric relation by expressing the offset and midpoint wavenumbers into shot and geophone wavenumbers and using the plane wave relation (1.6). The

stationary phase condition for MZO is transformed as follows:

$$\begin{aligned}
2h &= \frac{v^2 t_0 k_h}{4\omega}\left[\frac{1}{\sqrt{(1-\frac{vk_y}{2\omega})^2-(\frac{vk_h}{2\omega})^2}}+\frac{1}{\sqrt{(1+\frac{vk_y}{2\omega})^2-(\frac{vk_h}{2\omega})^2}}\right] \\
&= \frac{v(k_g-k_s)}{\omega}\frac{vt_0}{2}\left[\frac{1}{\sqrt{(2-\frac{v(k_g+k_s)}{\omega})^2-(\frac{v(k_g-k_s)}{\omega})^2}}+\frac{1}{\sqrt{(2+\frac{v(k_g+k_s)}{\omega})^2-(\frac{v(k_g-k_s)}{\omega})^2}}\right] \\
&= (\sin\beta-\sin\alpha)\frac{vt_0}{4}\left[\frac{1}{\sqrt{(1-\sin\alpha)(1-\sin\beta)}}+\frac{1}{\sqrt{(1+\sin\alpha)(1+\sin\beta)}}\right] \\
&= (\sin\beta-\sin\alpha)\frac{vt_0}{4}\left[\frac{\sqrt{(1+\sin\alpha)(1+\sin\beta)}+\sqrt{(1-\sin\alpha)(1-\sin\beta)}}{\cos\alpha\cos\beta}\right].
\end{aligned} \tag{1.13}$$

Unfortunately, more trigonometry is needed to put expression (1.13) into a suitable form. I couldn't find a quicker way to arrive at the final result (1.14), so the reader has to bear a little more. First I will prove that

$$2\cos\frac{\beta-\alpha}{2}=\sqrt{(1+\sin\alpha)(1+\sin\beta)}+\sqrt{(1-\sin\alpha)(1-\sin\beta)}$$

by using the equality

$$1\pm\sin 2u=(\sin u\pm\cos u)^2.$$

We have

$$\begin{aligned}
&\sqrt{(1+\sin\alpha)(1+\sin\beta)}+\sqrt{(1-\sin\alpha)(1-\sin\beta)}= \\
&= (\sin\frac{\alpha}{2}+\cos\frac{\alpha}{2})(\sin\frac{\beta}{2}+\cos\frac{\beta}{2})+(\sin\frac{\alpha}{2}-\cos\frac{\alpha}{2})(\sin\frac{\beta}{2}-\cos\frac{\beta}{2}) \\
&= (\cos\frac{\beta-\alpha}{2}+\sin\frac{\beta+\alpha}{2})+(\cos\frac{\beta-\alpha}{2}-\sin\frac{\beta+\alpha}{2}) \\
&= 2\cos\frac{\beta-\alpha}{2}.
\end{aligned}$$

Therefore the geometric condition in equation (1.13) is transformed as follows:

$$\begin{aligned}
2h &= \frac{vt_0}{4}\left[(\sin\beta-\sin\alpha)\frac{2\cos\frac{\beta-\alpha}{2}}{\cos\alpha\cos\beta}\right] \\
&= \frac{vt_0}{2}2\sin\frac{\beta-\alpha}{2}\cos\frac{\beta+\alpha}{2}\frac{\cos\frac{\beta-\alpha}{2}}{\cos\alpha\cos\beta} \\
&= \frac{vt_0}{2}\cos\frac{\beta+\alpha}{2}\frac{\sin\beta\cos\alpha-\sin\alpha\cos\beta}{\cos\alpha\cos\beta},
\end{aligned}$$

and choosing the appropriate signs for the angles we finally have:

$$\frac{vt_0}{2}\cos\frac{\beta+\alpha}{2}(\tan\alpha-\tan\beta)=2h. \tag{1.14}$$

Equation (1.14) represents the geometric condition for the MZO stationary phase. It can be reduced to the condition of the DSR equation if we observe from Figure 1.8 that

$$\frac{vt_0}{2}\cos\frac{\beta+\alpha}{2}=z. \tag{1.15}$$

The quantity $\frac{vt_0}{2}$ has the length of the segment X_0R, and represents the zero-offset ray, normal to the reflector. The angle $\frac{\beta+\alpha}{2}$ is equal to the angle of the dipping reflector θ. From Figure 1.8 we extract the relations:

$$\begin{aligned}\alpha &= \theta+i\\ \beta &= \theta-i,\end{aligned} \tag{1.16}$$

which can be also used to demonstrate equation (1.15).

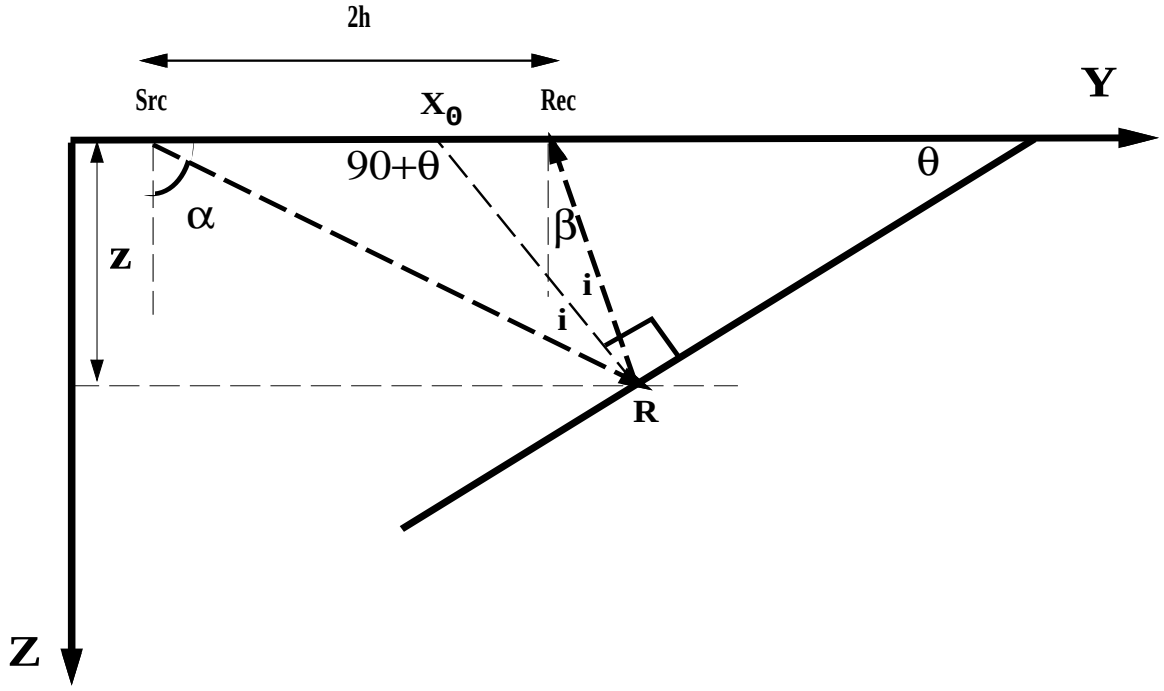

Figure 1.8: Geometric interpretation of the stationary phase condition for MZO. chapter2-MZOstapgeom [NR]

Equation (1.14) also provides a physical interpretation for the MZO operator. It relates the source-receiver traveltime to the zero-offset traveltime, the offset and the dip of the reflector. The zero-offset ray X_0R bisects the source-receiver ray and forms with each segment an incident angle i. At the same time the incident angle is constrained by equation (1.16) that connects the source angle α, the receiver angle β,

and the dipping reflector angle θ. The zero-offset ray therefore has to be perpendicular to the dipping reflector, bisect the source-receiver traveltime and has the length determined by the depth of the reflection point and the dip of the reflecting surface.

1.3 Separating the NMO and DMO corrections

For constant velocity we can further dissect the MZO equation (1.4) into DMO and NMO. The problem that arises in separating the NMO and DMO operators is deciding which order of separation is optimal. Applying the MZO operator directly to the prestack data for a common-offset section with offset h_0 generates straightway the zero-offset section

$$p(t, k_y, h = 0, z = 0) = \mathbf{MZO} \cdot p(t, k_y, h = h_0, z = 0),$$

but in practice the common procedure is to apply NMO first, then DMO. The procedure can be refined by doing inverse NMO followed by a new NMO correction. However, including this step does not illuminate the question of how to separate the DMO and NMO steps from MZO. The problem we face is that the two operators (NMO and DMO) do not commute, and thus it is necessary to define two different types of DMO operators: DMO applied after NMO (the standard method) and DMO applied before NMO (Gardner et al, 1986). Therefore MZO can be separated into two DMO and NMO sequences:

- $\mathbf{MZO} = \mathbf{DMO} \cdot \mathbf{NMO}$, the usual DMO.
- $\mathbf{MZO} = \mathbf{NMO} \cdot \mathbf{DMO}^*$.

To distinguish the two different DMO operators, the DMO before NMO operator is thereafter written with an asterisk: DMO*. Before separating the DMO operator, however, it is necessary to formally define an NMO operator.

1.3.1 The NMO and inverse NMO operators

An NMO operator can be defined as

$$p_{nmo}(t_n, k_y, h) = p(t(t_n, h), k_y, h), \tag{1.17}$$

where t_n represents the NMO-corrected traveltime

$$t_n^2 = t^2 - \frac{4h^2}{v^2},$$

and the field $p(t(t_n, h), k_y, h)$ represents the remapping (shifting) of the original common-offset field to the NMO-corrected field. This NMO formulation assumes spherical divergence was applied to the data to compensate for geometric spreading. We can

include the spherical divergence correction as an amplitude term in the NMO operator which then becomes:

$$p_{nmo}(t_n, k_y, h) = \frac{t}{t_n} p(t(t_n, h), k_y, h). \tag{1.18}$$

The presence of the amplitude term has a physical justification. The amplitude of the wavefield is higher at earlier traveltimes. In other words, the same event has a greater amplitude in a zero-offset section than in a common-offset section. Because the NMO times are smaller than the common-offset times, the amplitude of the field should be increased proportionally. This scheme assumes that no amplitude gain control or spherical divergence has been applied to the original wavefield. Otherwise, the amplitude term can simply be ignored.

To obtain the NMO-corrected field in the frequency domain, we Fourier transform the NMO equation (1.18) in time and change the integration variable from the NMO-corrected time t_n to the recording time t, as follows

$$\begin{aligned} p_{nmo}(\omega, k_y, h) &= \int dt_n \; e^{i\omega t_n} p_{nmo}(t_n, k_y, h) \\ &= \int dt_n \; e^{i\omega t_n} \frac{t}{t_n} p(t(t_n, h), k_y, h) \\ &= \int dt \; e^{i\omega \sqrt{t^2 - \frac{4h^2}{v^2}}} \frac{t^2}{t^2 - \frac{4h^2}{v^2}} p(t, k_y, h), \end{aligned} \tag{1.19}$$

noting that the change of variable eliminates the need to time-shift the prestack field from t to t_n, a shift that is now performed by the exponential multiplication. The Jacobian of the transformation $t_n \rightarrow t$, from equation (1.18), is

$$J = \left[\frac{dt_n}{dt} \right] = \frac{t}{t_n}.$$

Conversely, the inverse NMO (INMO) can be defined as

$$p(t, k_y, h) = \frac{t_n}{t} p_{nmo}(t_n(t, h), k_y, h), \tag{1.20}$$

where

$$t^2 = t_n^2 + \frac{4h^2}{v^2}.$$

In the Fourier domain, the INMO-corrected field becomes

$$\begin{aligned} p(\omega, k_y, h) &= \int dt \; e^{i\omega t} \frac{t_n}{t} p_{nmo}(t_n(t, h), k_y, h) \\ &= \int dt_n \; e^{i\omega \sqrt{t_n^2 + \frac{4h^2}{v^2}}} \frac{t_n^2}{t_n^2 + \frac{4h^2}{v^2}} p_{nmo}(t_n, k_y, h), \end{aligned} \tag{1.21}$$

where the Jacobian of the transformation $t \rightarrow t_n$ is

$$J^{-1} = \left[\frac{dt}{dt_n}\right] = \frac{t_n}{t}.$$

Having defined the NMO and INMO operators, we can now use them to separate DMO from MZO. The phase-shift formulation of the MZO from equation (1.4) is

$$p_0(t_0, k_y, h) = \int d\omega \; p(\omega, k_y, h) \int dk_h \; e^{-\frac{i}{2}\text{sign}(\omega)\left[\sqrt{(\omega - v_y)^2 - v_h^2} + \sqrt{(\omega + v_y)^2 - v_h^2}\right] t_0 - ihk_h}.$$

The two possible cases-the usual DMO after NMO, and DMO* before NMO-are discussed in sections 2.3 and 2.4, respectively.

1.4 DMO after NMO

In the case of DMO after NMO, we need to identify the NMO operation inside the MZO integral formula, since MZO is defined as

$$\textbf{MZO} = \textbf{DMO} \cdot \textbf{NMO},$$

and we can obtain the DMO operator from the general MZO equation (**??**). Starting with the MZO relation (**??**) discussed in the preceding chapter, we can compare it with the stationary-phase result obtained by Hale (1983). To bring equation (**??**) to a form similar to Hale's, a series of transformations is necessary. This section analyzes them in detail. At the end, I arrive at a stationary-phase approximation that matches Hale's almost exactly, with the exception of a minor amplitude term that comes from a different NMO Jacobian implementation.

Equation (**??**) has the form

$$p_0(t_0, k_y) = \int dk_h \int d\omega \; e^{-\frac{i}{2}\,\text{sign}(\omega)\left[\sqrt{(\omega - v_y)^2 - v_h^2} + \sqrt{(\omega + v_y)^2 - v_h^2}\right] t_0} p(\omega, k_y, k_h);$$

eliminating the integration in k_h, which images the zero-offset, gives us

$$p_0(t_0, k_y, k_h) = \int d\omega \; e^{-\frac{i}{2}\,\text{sign}(\omega)\left[\sqrt{(\omega - v_y)^2 - v_h^2} + \sqrt{(\omega + v_y)^2 - v_h^2}\right] t_0} p(\omega, k_y, k_h).$$

This form suggests a Stolt formulation of the algorithm, replacing the exponential phase with a new variable ω_0 defined as in equation (**??**):

$$\omega_0 = \frac{1}{2}\text{sign}(\omega)\left[\sqrt{(\omega - v_y)^2 - v_h^2} + \sqrt{(\omega + v_y)^2 - v_h^2}\right].$$

In the Stolt form, the MZO equation without the inverse Fourier transform in ω_0 becomes

$$p_0(\omega_0, k_y, k_h) = \left[\frac{d\omega}{d\omega_0}\right] p(\omega(\omega_0, k_y, k_h), k_y, k_h), \tag{1.22}$$

where the field $p(\omega(\omega_0, k_y, k_h), k_y, k_h)$ is remapped (interpolated) from the constantly sampled variable ω to new values of ω that depend on the variable ω_0. The remapping $\omega \rightarrow \omega(\omega_0, k_y, k_h)$ is similar to the interpolation in Stolt migration. My interpolation assumes that for each value of ω_0 we can find the appropriate value of ω, by applying the inverse of relation (??), or, in other words, that we can find the values of ω for regularly sampled values of ω_0.

To avoid the interpolation step, we can perform a slow Fourier transform in the initial stage of transforming the prestack data field along the time dimension, and map it directly onto the required ω_0 values. This procedure is similar to Ottolini's (1982) derivation of the radial trace migration equation or to the transformations needed to find a better Stolt interpolation algorithm in Popovici et al (1993). The MZO equation (1.22) becomes

$$p_0(\omega_0, k_y, k_h) = \left[\frac{d\omega}{d\omega_0}\right] \int dt\ e^{i\omega(\omega_0, k_y, k_h)t}\ p(t, k_y, k_h).$$

Lastly, to isolate separate common-offset sections, I employ the same technique used to separate the offset in equation (1.3):

$$\begin{aligned} p_0(\omega_0, k_y) &= \int dk_h \left[\frac{d\omega}{d\omega_0}\right] \int dt\ e^{i\omega(\omega_0, k_y, k_h)t} \int dh\ e^{-ik_h h} p(t, k_y, h) \\ &= \int dh \int dt\ p(t, k_y, h) \int dk_h \left[\frac{d\omega}{d\omega_0}\right] e^{i\omega(\omega_0, k_y, k_h)t - ik_h h}, \end{aligned}$$

and isolating the stacking step represented by the integration in h yields

$$p_0(\omega_0, k_y, h) = \int dt\ p(t, k_y, h) \int dk_h \left[\frac{d\omega}{d\omega_0}\right] e^{i\omega(\omega_0, k_y, k_h)t - ik_h h}, \tag{1.23}$$

where the kernel in k_h can be computed using a stationary-phase approximation. The algebra that describes all the necessary expansions appears in Appendix 2.B, with the following final result:

$$\begin{aligned} I(t, k_y, h, \omega_0) &= \int dk_h \left[\frac{d\omega}{d\omega_0}\right] e^{i\omega(\omega_0, k_y, k_h)t - ik_h h} \\ &\approx \frac{\sqrt{2\pi}(t^2 - \frac{4h^2}{v^2})(\frac{4{\omega_0}^2}{v^2} - k_y^2)^{\frac{1}{2}}}{\sqrt{\omega_0}\left[t^2 - \frac{4h^2}{v^2} + h^2\frac{k_y^2}{\omega_0^2}\right]^{\frac{5}{4}}} e^{i\omega_0\sqrt{t^2 - \frac{4h^2}{v^2} + h^2\frac{k_y^2}{{\omega_0}^2}} + i\,\mathrm{sign}(\omega_0)\frac{\pi}{4}}. \end{aligned} \tag{1.24}$$

Equation (1.24) has the same phase as Hale's DMO, or any other DMO defined in Fourier domain, a result we expected since there is no controversy regarding the kinematics of the different DMO operators in constant velocity media. On the other hand the amplitude term is different from the familiar DMO amplitude formulations, a result which is discussed in the following section.

1.4.1 True amplitude processing?

Equation (1.24) represents an important result that warrants some comments. Since the result was extracted directly from the wave-equation, without any approximations except the stationary-phase solution, I expected to obtain the same Jacobian for the DMO operator as the one obtained by Zhang(1988) and Black et al (1993). The expression of the "true amplitude" DMO kernel in the Zhang (1988) or Black et al (1993) formulation is:

$$I(t_n, k_y, h, \omega_0) = \frac{t_n(t_n^2 + 2h^2\frac{k_{y0}^2}{\omega_0^2})}{(t_n^2 + h^2\frac{k_{y0}^2}{\omega_0^2})^{\frac{3}{2}}} e^{\,i\omega_0\sqrt{t_n^2+h^2\frac{k_{y0}^2}{\omega_0^2}}}. \tag{1.25}$$

Equation (1.24) can be further transformed to bring it to a form more similar to (1.25) by dismissing the $\sqrt{2\pi}$ as it simplifies with the $1/\sqrt{2\pi}$ omitted from the Fourier transforms, and substituting $t^2 - \frac{4h^2}{v^2}$ by t_n^2. This substitution actually brings in another scaling factor as I will show in the next subsection, but that factor is not relevant in this discussion. After these substitutions equation (1.24) can be written as:

$$I(t_n, k_y, h, \omega_0) = \frac{t_n^2(\frac{4{\omega_0}^2}{v^2} - k_y^2)^{\frac{1}{2}}}{\sqrt{\omega_0}\left[t_n^2 + h^2\frac{k_y^2}{\omega_0^2}\right]^{\frac{5}{4}}} e^{\,i\omega_0\sqrt{t_n^2+h^2\frac{k_y^2}{{\omega_0}^2}}}. \tag{1.26}$$

By comparing the expressions (1.25) and (1.26) we see that the differences are irreconcilable, and that the "true amplitude" problem should be addressed at the start, in the DSR equation. I conclude the DSR equation is not "true amplitude" from a wave-equation point of view. I can only speculate on the reasons why there is such a discrepancy, since the DSR prestack migration equation (**??**) is derived from the constant-density constant-velocity wave equation and therefore there is no back-scattered energy created while propagating the seismic wavefield with this equation. Therefore, neglecting half of the wave field (the downgoing one) in the wave-equation solution, doesn't seem to be the source of conflict. It could also be that the imaging condition of setting the time and offset equal to zero can be improved. Jim Black suggested it is possible to work the analysis backwards, starting from the "true amplitude" form of the MZO or DMO equation and arrive at a DSR jacobian that will provide a wave-equation amplitude consistent DSR migration. In other words modify the downward continuation operator in the DSR migration equation by including a new amplitude term $W(\omega, k_y, k_h, z)$ as follows

$$p(t=0, k_y, h=0, z) = \int d\omega \int dk_h \; W(\omega, k_y, k_h, z)\; e^{ik_z(\omega,k_y,k_h)z} p(\omega, k_y, k_h, z=0).$$

1.4.2 The relation between MZO and Hale's DMO

Comparing equation (1.24) with Hale's stationary-phase approximation of DMO (equation 3.16a in Hale, 1983),

$$I_H(t_n,k_y,h,\omega_0) \approx \frac{\sqrt{2\pi}t_n^2(\frac{4{\omega_0}^2}{v^2}-k_y^2)^{\frac{1}{2}}}{\sqrt{\omega_0}\left[t_n^2+h^2\frac{k_y^2}{\omega_0^2}\right]^{\frac{5}{4}}}e^{i\omega_0\sqrt{t_n^2+h^2\frac{k_y^2}{{\omega_0}^2}}+i\mathrm{sign}(\omega_0)\frac{\pi}{4}}, \tag{1.27}$$

shows that they are essentially the same expression, a result we expected. The expression

$$t^2-\frac{4h^2}{v^2}$$

in equation (1.27) has simply been replaced by the NMO-corrected time t_n^2. However, Hale considers the NMO-corrected field $p_n(t_n,k_y,h)$ in his evaluation of the stationary-phase approximation of the DMO kernel, and depending on the definition of NMO used, slight differences may appear in the evaluation of equation (1.23). Hale's DMO stationary-phase approximation is

$$p_0(\omega_0,k_y,h)=\int dt_n p_n(t_n,k_y,h)I_H(t_n,k_y,h,\omega_0), \tag{1.28}$$

while the MZO stationary-phase approximation is

$$p_0(\omega_0,k_y,h)=\int dt\ p(t,k_y,h)I(t,k_y,h,\omega_0). \tag{1.29}$$

By transforming the variable of integration in equation (1.29) from t to t_n, and using the Jacobian

$$\left[\frac{dt}{dt_n}\right]=\frac{t_n}{t},$$

we get

$$p_0(\omega_0,k_y,h)=\int dt_n\frac{t_n}{t}p(t(t_n,h),k_y,h)I(t_n,k_y,h,\omega_0), \tag{1.30}$$

where the field $p(t(t_n,h),k_y,h)$ is the original prestack data NMO-corrected. If the NMO operator is defined without any Jacobian, we can stop here, and the only difference from Hale's DMO is the factor $\frac{t_n}{t}$. However, when we use the NMO definition in equation (1.18)

$$p_{nmo}(t_n,k_y,h)=\frac{t}{t_n}p(t(t_n,h),k_y,h),$$

which is different from Hale's

$$p_{nmo}(t_n,k_y,h)=\frac{t_n}{t}p(t(t_n,h),k_y,h),$$

and the DMO stationary-phase approximation becomes

$$p_0(\omega_0,k_y,h)=\int dt_n\frac{t_n^2}{t^2}p_n(t_n,k_y,h)I(t_n,k_y,h,\omega_0). \tag{1.31}$$

Hale's DMO using a different Jacobian for the NMO cancels the Jacobian from the transformation of the integration variable ($t \rightarrow t_n$). The Jacobian used in equation (1.18) is justified when no spherical divergence correction has been applied to the data. (If spherical divergence has been applied, then the Jacobian loses its physical sense, and the NMO transformation becomes just a time-shift, without any amplitude correction. In this case, the DMO integral has just the $\frac{t_n}{t}$ amplitude correction term.) Therefore, the final DMO equation is

$$p_0(\omega_0, k_y, h) = \int dt_n p_n(t_n, k_y, h) \frac{\sqrt{2\pi} t_n^4 (\frac{{\omega_0}^2}{v^2} - k_y^2)^{\frac{1}{2}}}{\sqrt{\omega_0}(t_n^2 + \frac{4h^2}{v^2}) \left[t_n^2 + h^2 \frac{k_y^2}{\omega_0^2}\right]^{\frac{5}{4}}} e^{i\omega_0 \sqrt{t_n^2 + h^2 \frac{k_y^2}{{\omega_0}^2}} + i \mathrm{sign}(\omega_0) \frac{\pi}{4}}. \tag{1.32}$$

The key amplitude term in equation (1.32) is:

$$(\frac{{\omega_0}^2}{v^2} - k_y^2)^{\frac{1}{2}}. \tag{1.33}$$

The existence condition for the square root acts as a dip filter in the frequency-wavenumber domain. This filter cuts out the evanescent energy, events with impossible dip for a given velocity. While the effect of such events prevents noise with impossible dip to enter the final image, it can be argued that when the velocity is not known, some legitimate events could be filtered out. Hale's DMO by Fourier transform does not use the velocity cutoff filter, as equation (**??**) confirms. The left panel in Figure 1.9 shows the impulse response of the DMO by Fourier transform. In contrast to Hale's DMO, the stationary-phase implementation of DMO given by equation (1.32) illustrated by the middle panel in Figure 1.9, applies a velocity cutoff to the evanescent events. However, if we omit the dip filter term (1.33) in equation (1.32), we obtain the operator displayed in the right panel in Figure 1.9.

1.5 DMO before NMO

In the case of DMO* before NMO, the MZO operator is defined as

$$\mathbf{MZO} = \mathbf{NMO} \cdot \mathbf{DMO}^*,$$

and the DMO* operator can be obtained by isolating the NMO operator in equation (1.23). Using the definition of the NMO in equation (1.19), I rewrite equation (1.23) as

$$p_0(\omega_0, k_y, h) = \int dt\ p(t, k_y, h)\ e^{i\omega_0 \sqrt{t^2 - \frac{4h^2}{v^2}}} \frac{t^2}{t^2 - \frac{4h^2}{v^2}} I(t, k_y, h, \omega_0)\ e^{-i\omega_0 \sqrt{t^2 - \frac{4h^2}{v^2}}} \frac{t^2 - \frac{4h^2}{v^2}}{t^2},$$

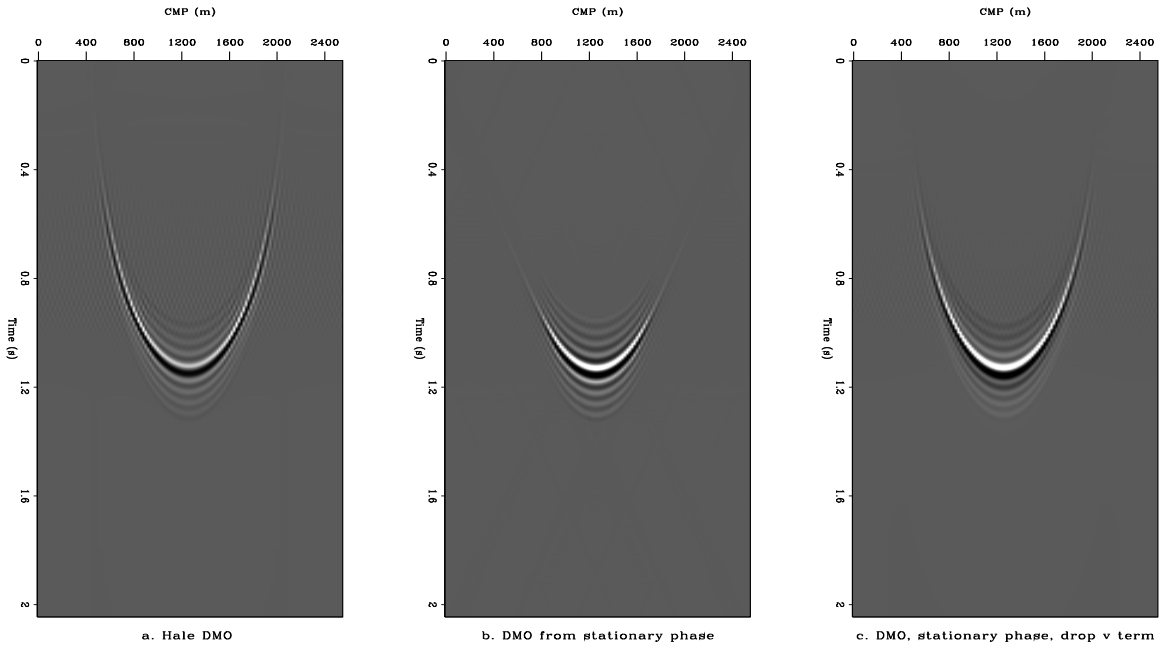

Figure 1.9: Impulse responses for several implementations of the DMO operator.
a. Hale's DMO by Fourier transform.
b. The stationary-phase DMO given by equation 1.32.
c. The stationary-phase DMO without the dip filtering term 1.33. chapter2-C2f123
[ER]

where $I(t, k_y, h, \omega_0)$ represents the stationary phase approximation from (1.24). The kernel for the DMO^* operator becomes

$$I(t, k_y, h, \omega_0) = \frac{\sqrt{2\pi}(t^2 - \frac{4h^2}{v^2})^2(\frac{4{\omega_0}^2}{v^2} - k_y^2)^{\frac{1}{2}}}{t^2\sqrt{\omega_0}\left[t^2 - \frac{4h^2}{v^2} + h^2\frac{k_y^2}{\omega_0^2}\right]^{\frac{5}{4}}} e^{i\omega_0\sqrt{t^2 - \frac{4h^2}{v^2} + h^2\frac{k_y^2}{{\omega_0}^2}} - i\omega_0\sqrt{t^2 - \frac{4h^2}{v^2}} + i\,\mathrm{sign}(\omega_0)\frac{\pi}{4}}. \tag{1.34}$$

1.5.1 The kinematics of the DMO-before-NMO operator

The DMO* applied before NMO is similar to the DMO described by Gardner et al. (1986) and Forel and Gardner (1988). Because it is less usual than the DMO after NMO operator, it is important to examine its behavior and the kinematics. As mentioned earlier, to distinguish between the two types of DMO operators, I designate the DMO operator applied before NMO as DMO* (with an asterisk).

The parametric equation (??) for the MZO, given in the introduction, is

$$\begin{cases} x_0 = \dfrac{2h^2 \sin\theta}{v\sqrt{t_h^2 - \frac{4h^2}{v^2}\cos^2\theta}} \\ \\ t_0 = \dfrac{t_h^2 - \frac{4h^2}{v^2}}{\sqrt{t_h^2 - \frac{4h^2}{v^2}\cos^2\theta}}, \end{cases}$$

where t_h is the time from source to receiver, h is the offset equal to half the distance between source and receiver, v is the medium velocity, and θ is the dip of the reflector.

The time t_0 represents the zero-offset time after the NMO and DMO corrections (or in one-step MZO). To apply DMO* before NMO, we isolate the NMO correction

$$t_0^2 = t_d^2 - \frac{4h^2}{v^2},$$

where t_d is the traveltime after the DMO* correction. Alternatively, we can find the DMO* traveltimes directly by replacing t_d in equation (??), as follows:

$$\begin{aligned} t_d^2 &= t_0^2 + \frac{4h^2}{v^2} \\ &= \frac{(t_h^2 - \frac{4h^2}{v^2})^2 + \frac{4h^2}{v^2}(t_h^2 - \frac{4h^2}{v^2}\cos^2\theta)}{t_h^2 - \frac{4h^2}{v^2}\cos^2\theta} \\ &= \frac{t_h^4 - \frac{4t_h^2h^2}{v^2} + \frac{16h^4}{v^4}\sin^2\theta}{t_h^2 - \frac{4h^2}{v^2}\cos^2\theta}. \end{aligned} \tag{1.35}$$

Combined with the expression for the surface coordinate x_0, the parametric equations for DMO* are

$$\begin{cases} x_0 = \dfrac{2h^2 \sin\theta}{v\sqrt{t_h^2 - \frac{4h^2}{v^2}\cos^2\theta}} \\ \\ t_d = \dfrac{\sqrt{t_h^4 - \frac{4t_h^2h^2}{v^2} + \frac{16h^4}{v^4}\sin^2\theta}}{\sqrt{t_h^2 - \frac{4h^2}{v^2}\cos^2\theta}}. \end{cases} \tag{1.36}$$

The result of applying the DMO* operator to a constant-offset diffraction curve appears in Figure 1.10. The left panel in Figure 1.10a, shows the effect of the DMO* operator applied to a constant-offset diffraction curve. The asterisks mark the location of the zero-offset diffraction curve, shifted in time with NMO correction $\frac{4h^2}{v^2}$. Applying NMO to this curve will bring it to the correct zero-offset location. On the right, Figure 1.10b shows the effect of the same DMO* operator on a constant-offset diffraction curve, using a wavelet and constant amplitude along the DMO* curve. A better amplitude along the DMO* operator is obtained by using the kernel (1.34).

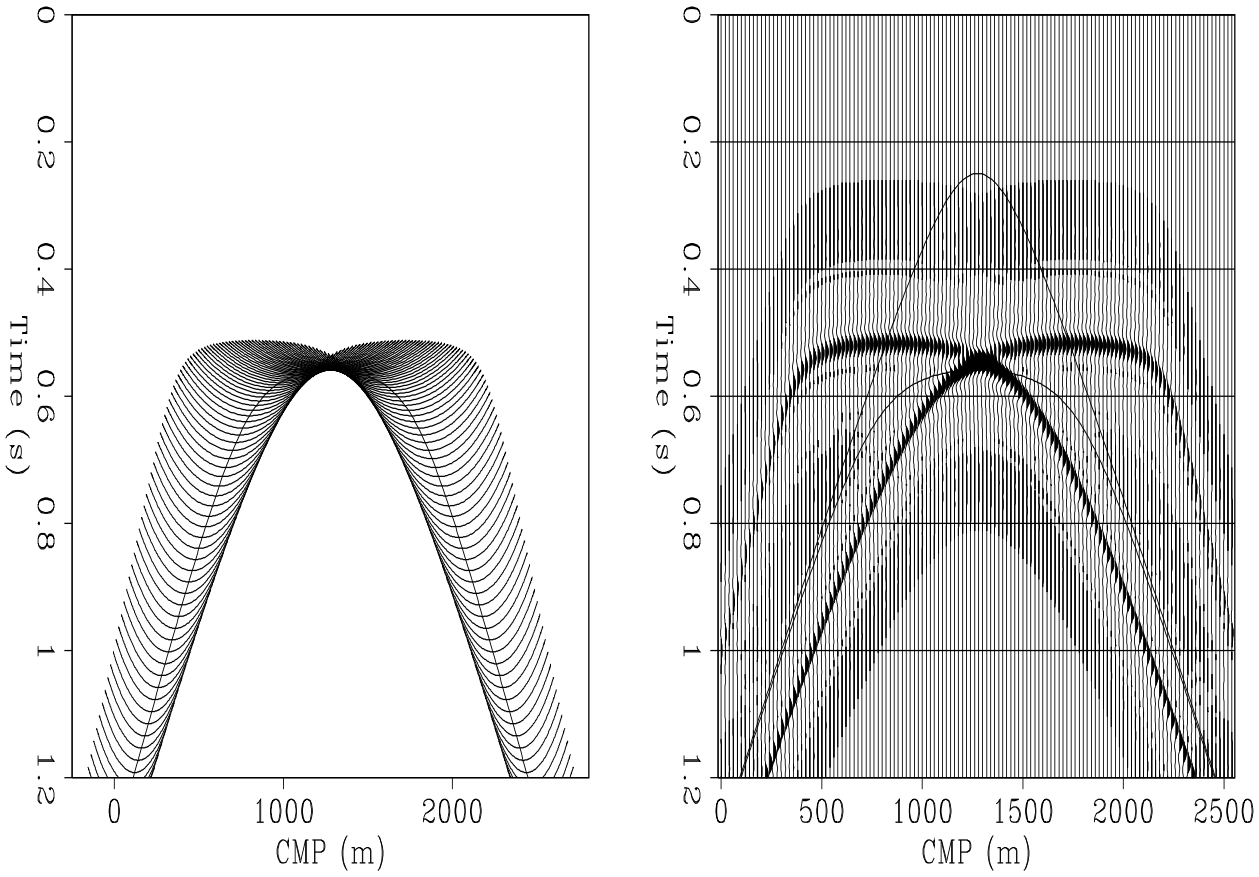

Figure 1.10: $NMO \cdot DMO$ transforms a common-offset diffraction curve to a zero-offset hyperbola.
a. DMO* kinematics; each point on the common-offset diffraction curve is spread along the DMO* curve. The asterisks represent the zero-offset diffraction curve shifted down with the inverse NMO correction ($\frac{4h^2}{v^2}$).
b. The result of applying DMO* to the common-offset diffraction curve. The artifacts are the result of using a constant amplitude along the DMO curve. chapter2-C2f6 [ER]

By eliminating the parameter $\sin\theta$ between the two relations in (1.36) we arrive at Gardner's DMO formulation:

$$t_d^2 = (t_h^2 - \frac{4h^2}{v^2})(1 - \frac{x_0^2}{h^2}) + \frac{4h^2}{v^2}, \tag{1.37}$$

which is simply the usual DMO shifted down with the NMO correction.

1.6 Appendix 2.A: Stationary-phase computation for MZO

Migration to zero-offset for separate common-offset sections requires the computation of the kernel (1.2)

$$I(\omega, k_y; t_0, h_0) = \int dk_h \; e^{i\omega_0(\omega, k_y, k_h)t_0 - ik_h h_0},$$

where the phase of the exponential is

$$\phi(k_h) = -\frac{vt_0}{4}\text{sign}(\omega)\left[\sqrt{(\frac{2\omega}{v} - k_y)^2 - k_h^2} + \sqrt{(\frac{2\omega}{v} + k_y)^2 - k_h^2}\right] - k_h h_0. \qquad (1.38)$$

The kernel can be computed numerically by integrating for all values of k_h, at a very high computational cost, or by finding a stationary-phase approximation for it.

Integrals of the form

$$I(k) = \int_{-\infty}^{\infty} e^{ik\phi(t)} f(t)\, dt \qquad (1.39)$$

are approximated asymptotically (Zauderer, 1989) when $k \to \infty$ by

$$I(k) \approx \left[\frac{2\pi}{k \mid \phi''(t_0) \mid}\right]^{\frac{1}{2}} f(t_0) e^{ik\phi(t_0) + \text{sign}(\phi''(t_0))\frac{i\pi}{4}};$$

t_0 is the stationary point where the derivative of the phase is zero, k is a large real parameter, $f(t)$ is a real or complex function, and the real valued function $\phi(t)$ is the *phase term*. The stationary-point approximation is based on finding the major contribution to the integral in the neighborhood of the stationary point, by expanding $f(t)$ and $\phi(t)$ in a Taylor series around t_0. The approximation described here assumes that the second derivative is nonzero, which is the situation in the MZO case. If the integral (1.39) is defined on a closed interval, the contribution of the point of stationary phase, t_0, to the integral is more important than the contribution of the end points. Integration by parts shows the contribution of the end points to be $O(\frac{1}{k})$ if the derivative of the phase is not zero at the end points (Erdelyi, 1956).

In order to evaluate the stationary point for the phase (1.38), we need to find the roots of the equation

$$\phi'(k_h) = -h_0 + \frac{vt_0}{4}\text{sign}(\omega)k_h\left[\frac{1}{\sqrt{(\frac{2\omega}{v} - k_y)^2 - k_h^2}} + \frac{1}{\sqrt{(\frac{2\omega}{v} + k_y)^2 - k_h^2}}\right]. \qquad (1.40)$$

The second derivative of the phase is nonzero, since it consists of the sum of four positive terms multiplied by $\frac{vt_0}{4}\text{sign}(\omega)$, as follows:

$$\begin{aligned}\phi''(k_h) &= \frac{vt_0}{4}\text{sign}(\omega)\left[\frac{1}{\sqrt{(\frac{2\omega}{v}-k_y)^2-k_h^2}}+\frac{1}{\sqrt{(\frac{2\omega}{v}+k_y)^2-k_h^2}}+\right.\\ &+ \left.\frac{k_h^2}{[(\frac{2\omega}{v}-k_y)^2-k_h^2]^{\frac{3}{2}}}+\frac{k_h^2}{[(\frac{2\omega}{v}+k_y)^2-k_h^2]^{\frac{3}{2}}}\right] \qquad (1.41)\\ &= \frac{vt_0}{4}\text{sign}(\omega)\frac{(\frac{2\omega}{v}-k_y)^2}{[(\frac{2\omega}{v}-k_y)^2-k_h^2]^{\frac{3}{2}}}+\frac{(\frac{2\omega}{v}+k_y)^2}{[(\frac{2\omega}{v}+k_y)^2-k_h^2]^{\frac{3}{2}}}\end{aligned}$$

The fact that the second derivative is nonzero ensures that the curvature does not change, and that the phase always has a maximum or a minimum and therefore a stationary point. Figure /FIGApp1 shows the phase function at several time levels for a fixed pair of values ω, k_y. The sign of ω determines whether the phase is positive or negative.

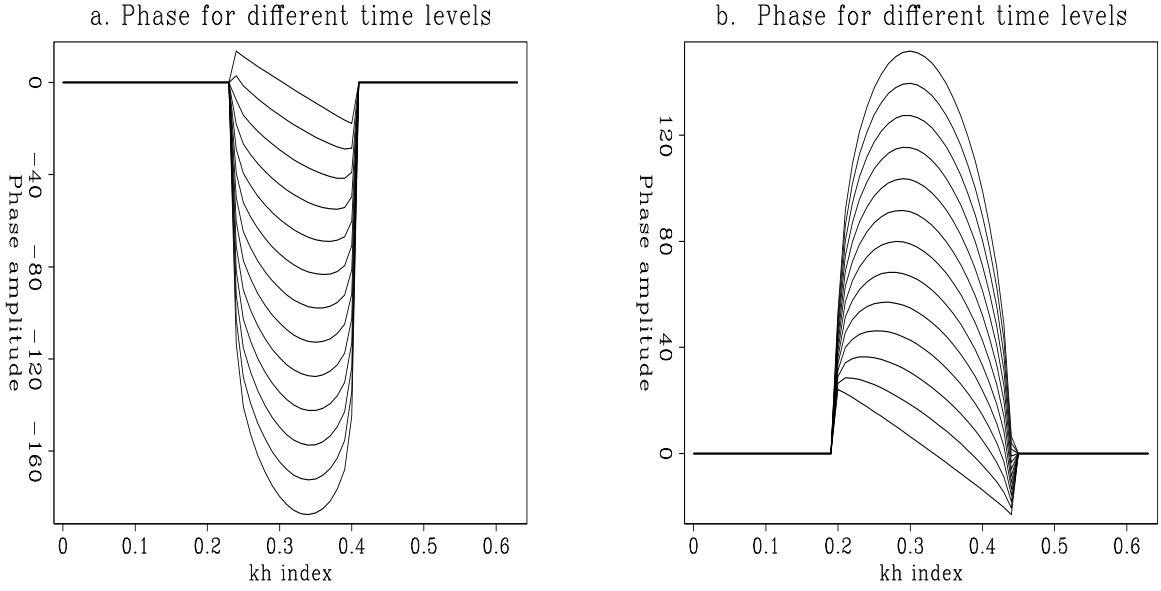

Figure 1.11: Plot of the phase function for a constant pair of values ω, k_y. The different plots correspond to increasing depth levels.
a. Phase corresponding to positive ω.
b. Phase corresponding to negative ω. chapter2-App1 [ER]

1.7 Appendix 2.B: Stationary-phase algebra for standard DMO

In this appendix, using the stationary-phase approximation, I evaluate the integral

$$I(t,k_y,h,\omega_0)=\int dk_h \left[\frac{d\omega}{d\omega_0}\right] e^{i\omega(\omega_0,k_y,k_h)t-ik_hh},$$

where the Jacobian, as computed previously in equation (**??**), is

$$\left[\frac{d\omega}{d\omega_0}\right]=(1+\frac{v^2k_h^2}{4{\omega_0}^2-v^2k_y^2})^{-\frac{1}{2}}\left[1-\frac{v^4k_h^2k_y^2}{(4{\omega_0}^2-v^2k_y^2)^2}\right],$$

and the phase $\omega(\omega_0,k_y,h)t-k_hh$ is

$$\Phi=\omega_0\left[1+\frac{v^2k_h^2}{4{\omega_0}^2-v^2k_y^2}\right]^{\frac{1}{2}}t-k_hh.$$

The stationary point $\bar{k_h}$ occurs at the point where the derivative of the phase $\Phi(k_h)$ is zero. Setting the derivative of Φ to zero yields the equation

$$\frac{v^2k_h\omega_0t}{4{\omega_0}^2-v^2k_y^2}\left[1+\frac{v^2k_h^2}{4{\omega_0}^2-v^2k_y^2}\right]^{-\frac{1}{2}}=h,$$

which has the solution

$$\tilde{k_h}=\frac{h(4{\omega_0}^2-v^2k_y^2)}{v^2\sqrt{{\omega_0}^2(t^2-\frac{4h^2}{v^2})+h^2k_y^2}}.$$

Inserting the value of $\tilde{k_h}$ in the expression of the phase Φ, we have

$$\Phi(\tilde{k_h})=\omega_0\sqrt{(t^2-\frac{4h^2}{v^2})+h^2\frac{k_y^2}{\omega_0^2}}.$$

The second derivative of the phase is also needed, for several reasons. First, the sign of the $\frac{\pi}{4}$ term depends on the sign of the second derivative. Second, the amplitude term includes the second derivative evaluated at the stationary point. And third, the stationary-phase approximation is based on the assumption that the second derivative of the phase is different from zero at the stationary point. The expression of the second derivative is

$$\Phi''=\frac{\omega_0t(\frac{4{\omega_0}^2}{v^2}-k_y^2)^{\frac{1}{2}}}{(\frac{4{\omega_0}^2}{v^2}-k_y^2+k_h^2)^{\frac{3}{2}}}.$$

Evaluating the second derivative Φ'' at the stationary point $\tilde{k_h}$ gives us

$$\Phi''(\tilde{k_h})=\frac{(t^2-\frac{4h^2}{v^2}+\frac{h^2k_y^2}{\omega_0^2})^{\frac{3}{2}}}{t^2(\frac{4{\omega_0}^2}{v^2}-k_y^2)},$$

and the Jacobian evaluated at $\tilde{k_h}$ is

$$\left[\frac{d\omega}{d\omega_0}\right]_{k_h=\tilde{k_h}} = \frac{t^2 - \frac{4h^2}{v^2}}{t\sqrt{t^2 - \frac{4h^2}{v^2} + h^2\frac{k_y^2}{\omega_0^2}}}.$$

Finally, multiplying all the terms produces the following stationary-phase approximation of the initial kernel:

$$I(t, k_y, h, \omega_0) \approx \frac{\sqrt{2\pi}(t^2 - \frac{4h^2}{v^2})(\frac{4{\omega_0}^2}{v^2} - k_y^2)^{\frac{1}{2}}}{\sqrt{\omega_0}\left[t^2 - \frac{4h^2}{v^2} + h^2\frac{k_y^2}{\omega_0^2}\right]^{\frac{5}{4}}} e^{i\omega_0\sqrt{t^2 - \frac{4h^2}{v^2} + h^2\frac{k_y^2}{{\omega_0}^2}} + i\,\mathrm{sign}(\omega_0)\frac{\pi}{4}}.$$